Yield Precursor Dislocation Avalanches in Small Crystals: The Irreversibility Transition

Xiaoyue Ni, 1,* Haolu Zhang, Danilo B. Liarte, Louis W. McFaul, Karin A. Dahmen, 1 James P. Sethna,² and Julia R. Greer¹

¹Division of Engineering and Applied Sciences, California Institute of Technology, Pasadena, California 91125, USA ²Laboratory of Atomic and Solid State Physics, Cornell University, Ithaca, New York 14853-2501, USA ³Physics Department, University of Illinois at Urbana-Champaign, Urbana, Illinois 61801, USA

(Received 29 November 2018; revised manuscript received 5 June 2019; published 15 July 2019)

The transition from elastic to plastic deformation in crystalline metals shares history dependence and scale-invariant avalanche signature with other nonequilibrium systems under external loading such as colloidal suspensions. These other systems exhibit transitions with clear analogies to work hardening and yield stress, with many typically undergoing purely elastic behavior only after "training" through repeated cyclic loading; studies in these other systems show a power-law scaling of the hysteresis loop extent and of the training time as the peak load approaches a so-called reversible-to-irreversible transition (RIT). We discover here that deformation of small crystals shares these key characteristics: yielding and hysteresis in uniaxial compression experiments of single-crystalline Cu nano- and micropillars decay under repeated cyclic loading. The amplitude and decay time of the yield precursor avalanches diverge as the peak stress approaches failure stress for each pillar, with a power-law scaling virtually equivalent to RITs in other nonequilibrium systems.

DOI: 10.1103/PhysRevLett.123.035501

The mechanical deformation of macroscopic metals is usually characterized by the yield stress, below which the metal responds elastically, and beyond which plastic deformation is mediated by complex dislocation motion and interactions. In small-scale crystals, dislocation activities manifest as avalanches, with characteristic discrete strain bursts in the stress-strain response of the sample [1–3]. The avalanches exhibit complex scale invariant behavior on wide length scales and timescales [3,4]. The yield stress depends on the history of the sample: if the sample were unloaded and then reloaded during plastic flow, the previous maximum stress would become the current yield stress, below which there are no deviations from linear-elastic response, with the flow and yield stresses always increasing, i.e., work hardening [5]. The elastic-to-plastic transition in crystals finds theoretical analogies to many nonequilibrium material systems [6]: dilute colloidal suspensions [7,8], plastically deformed amorphous solids [9–12], granular materials [13–15], and dislocation-based simulations of crystals [16]. In all these other systems, the loading-unloading hysteresis disappears only after repeated cycling to the maximum stress, coined as material training. These systems exhibit power laws and scaling in the limit that the maximum stress approaches a critical value, the so-called reversible-irreversible transition (RIT), which separates trainable and untrainable regimes. For crystals, the nonelastic reloading behavior is in reminiscence of fatigue, in which plastic training is characterized by cyclic strain hardening, an evolution of hysteresis loops, and the emergence of well-defined dislocation microstructures [17,18]. However, the immediate elastic-nonelastic asymmetry in the unloading-reloading process lies in the realm of abnormal fatigue behavior, such as the anomalous Bauschinger effect, which has only been observed before in polycrystalline metals [19], in small system sizes with unconventional microstructures [20–23] or in the presence of strong strain gradients [24], or in single crystals during the initial elastic loading [25]. In this Letter, we discover that sub-micron- and micron-sized metals display the same RIT, with the training hysteresis reduced in larger sample volumes. We begin by showing that the "textbook description" of yield stress and work hardening is fundamentally violated even for metallic single-crystalline micro- and nanopillars under uniaxial plastic deformation.

Figure 1(a) shows typical true stress-strain responses of displacement-controlled (DC) compression of singlecrystalline (111)-oriented Cu nanopillars with diameters of 300 nm, 500 nm, 700 nm, 1 μ m, and 3 μ m. This plot reveals multiple discrete strain bursts, which have been shown to correspond to dislocation avalanches that are triggered from depinning events during plastic flow [26]. Some occasional strain bursts are also present during the post-avalanche reloading processes at stresses lower than the current "yield stress," which is defined as the previous maximum stress that triggered the most-recent avalanche unloading event, exemplified in Fig. 1(b) for the 300 nm diameter pillar test. The presence of such preyield avalanches contrasts with the conventional definition of history-dependent yield point in metals that strictly separates the purely elastic behavior upon unloading and

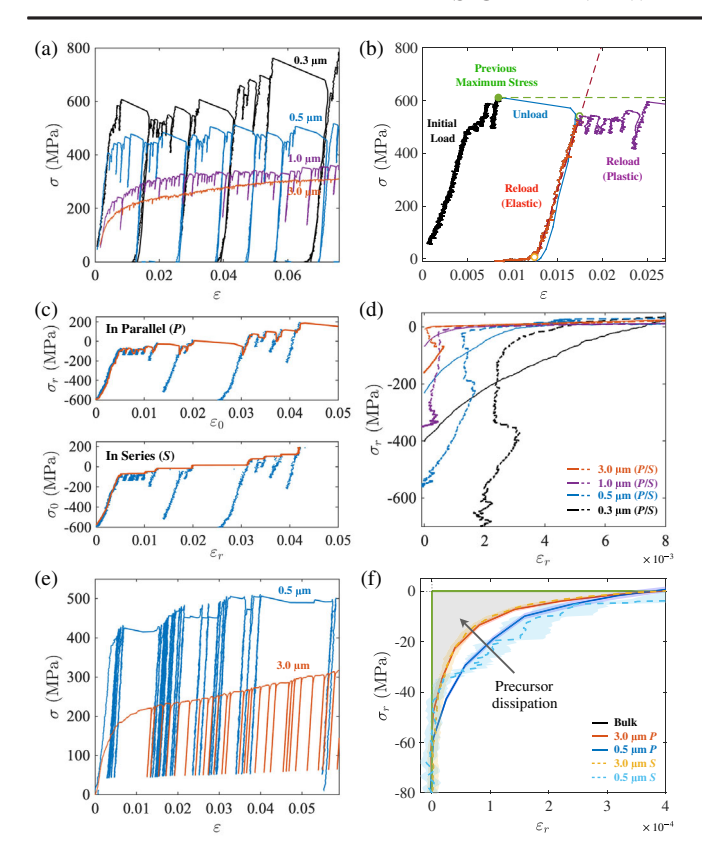


FIG. 1. Precursor avalanches present in the uniaxial quasistatic and unload-reload cyclic compression experiments on single crystalline Cu pillars. (a) Representative stress-strain data for displacement-controlled (DC) compression experiments on different diameter pillars. (b) A close-up of the first fast-avalanche induced unloading-reloading process in the 300 nm diameter pillar DC compression test. The first reloading starts to deviate from the linear elastic response at a strain of ~ 0.017 , while at a stress lower than the updated "yield stress," defined as the previous maximum stress. (c) The in-parallel (P) stress (σ_r) and in-series (S) strain (ε_r) reconstruction of the reloading process marked in (b), where dots and solid lines represent raw and interpolated data separately. (d) The non-Hookean reconstruction results obtained from displacement-controlled tests on seven identically prepared pillars for each size of micropillars. (e) Sample stress-strain and (f) the reconstructed non-Hookean stress-strain data for two representative load-controlled (LC) unload-reload compression experiments on 3 um and 500 nm diameter pillars. The area of the shaded region represents the precursor dissipation for 3 μ m pillars.

reloading from irreversible plasticity. The plastic strain that occurs below the previous maximum stress is the yield-precursor strain.

As the occurrence of avalanches upon reloading is stochastic in small-scale crystals, we apply two types of stress-strain reconstruction to average all the reloading curves as a measure of the ensemble precursor deviation from the "peak stress" yielding. Figure 1(c) demonstrates the in-series and in-parallel reconstruction using the reloading process marked in Fig. 1(b). We first shift the origin of

each reloading process such that the stress is zeroed at the previous maximum stress and the strain is zeroed at the beginning. We interpolate and average the reloading response σ_r (in parallel) or stress ε_r (in series), along the monotonically increasing strain ε_0 (in parallel) or stress σ_0 (in series). Figure 1(d) shows the reconstruction results obtained from displacement-controlled tests on seven identically prepared pillars for each size of micropillars. We have subtracted the elastic strain to emphasize the plastic precursor behavior (see Supplemental Material, Sec. S2, for details of the reconstruction procedure [27]).

In the experiments presented here, larger precursor strain is prevalently observed in smaller pillars. However, we observe that the larger pillars that are monotonically loaded under displacement control generally produce shorter avalanche strains [37,38] and are less frequently spontaneously unloaded by the instrument compared with the smaller pillars. The emergent effect of system size on precursor avalanche behavior, where "system size" refers to the overall pillar volume, might arise from the variable unloading conditions. We conduct load-controlled (LC) compression experiments with several prescribed unloadreload cycles interrupting the quasistatic compression to investigate the size effect. The maximum stress increases 5 MPa per cycle, which equals to a quasistatic ramping rate of ~1.4 MPa/s. Figure 1(e) shows such unload-reload stress-strain response of representative 500 nm and 3 μ m diameter Cu pillars, and Fig. 1(f) compares their reconstructed yield-precursor stress-strain response. The types of precursor avalanches that we observe during the deformation of small micropillars that extend over $\sim 10^{-4}$ strains at precursor stresses that are ~5\% (20 MPa) lower than the previous maximum stress (~400 MPa) would pose significant corrections to Hookean elastic behavior if they persisted to macroscopic systems.

We numerically evaluate the energy dissipation per volume reduced by precursor avalanches in comparison with the conventional plastic behavior, the precursor dissipation, from an integral over the reconstructed stressstrain hysteresis, $U = -\int \sigma_r d\epsilon_0$, indicated by the shaded area in Fig. 1(f) for 3 μ m diameter samples. We observe larger precursor dissipation of ~60 kPa in the smaller 500 nm diameter pillars than the ~4 kPa in the larger 3 μ m diameter samples, which suggests that the precursor avalanches may disappear in macroscopic samples. This is different from finite-size effect in statistically averaged distributions, where individual avalanches are hard to resolve in bulk or in high-symmetry crystals [39]. Since we measure the ensemble hysteresis, which is in nature a sum of the dissipation, small avalanches below the resolution of the instrument will still be properly incorporated. Perhaps this explains why precursor avalanches have not been thoroughly examined in existing literature.

We conduct LC cyclic training experiments to study how the precursor hysteresis changes under repeated loading to

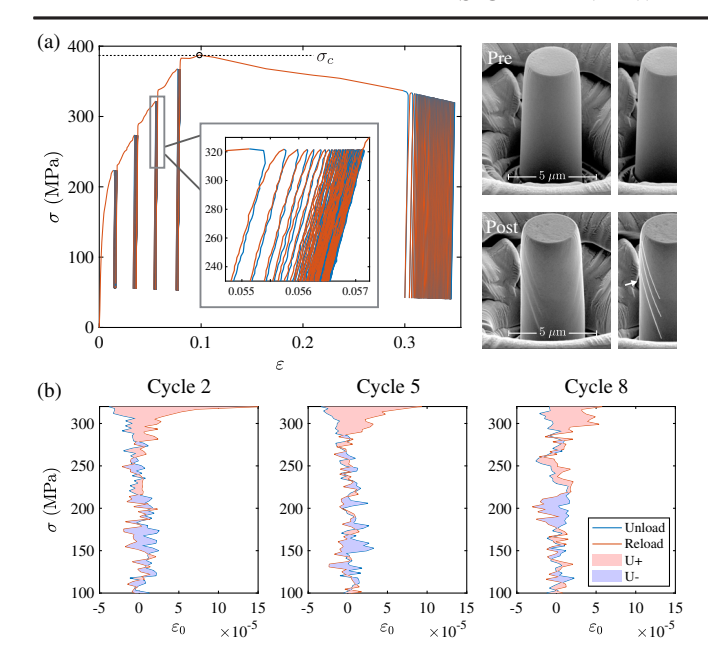


FIG. 2. Precursor avalanches trained over cyclic loading in micropillars. (a) Left: Estimated true stress-strain response from an LC training experiment on a 3 μ m diameter Cu pillar. Unloading and reloading stress-strain curves are marked in blue and red, respectively. The maximum stress is increased in five steps; the fifth step reaches the failure stress σ_c . At each step, 100 unload-reload cycles are prescribed. Right: pre- and post-test scanning electron microscope (SEM) images of this sample with the arrow and dashed line denoting the crystallographic slip lines on parallel planes characteristic of dislocation avalanches and glide in the enlarged images on the side. (b) The drift-corrected stress vs strain (see Supplemental Material, Sec. S4, for details [27]) during the second, fifth, and eighth cycles from data shown in (a) loaded to a maximum of ~340 MPa. Shaded area represents the energy dissipated through precursor avalanches, which decreases over cyclic loading.

the same maximum stress, analogous to experiments on other nonequilibrium systems [7,8]. We choose $3 \mu m$ diameter single crystalline Cu pillars as the primary experimental system because it is sufficiently large amongst the "small-scale" counterparts to exhibit failure under quasistatic loading as well as relatively deterministic precursor avalanche behavior. Figure 2(a) shows the estimated true stressstrain data from one representative training experiment on the left along with the scanning electron microscope (SEM) images of a typical pillar pre- and postcompression on the right. The failure stress, σ_c , or the stress beyond which the samples are no longer able to support additional applied load, is defined as the global maximum stress at \sim 390 MPa. Above this stress, the sample continually deforms plastically at a constant stress [40]. In the representative experiment, we prescribe five cyclic stress steps with maximum engineering stress from 228 MPa ($\sim 0.57\sigma_c$) to 452 MPa ($\sim 1.15\sigma_c$) at equal intervals of 56 MPa ($\sim 0.14\sigma_c$). In each stress step, we apply 100 unload-reload cycles, during which the sample is loaded to the same maximum stress and unloaded to a minimum of 56 MPa to maintain contact between the compression tip and the sample. We investigate the yield precursor dissipation evolution over all cycles at each stress step. Figure 2(b) shows the second, fifth, and eighth cycles of drift-corrected data (see Supplemental Material, Sec. S4, for details [27]) cycled to ~320 MPa in Fig. 2(a), with precursor dissipation indicated by the shaded areas.

We apply the multistep cyclic load function spanning the stress range $0.5-1.0\sigma_c$ to 24 identically prepared samples. It is reasonable to assume that for a cycle at a specific maximum stress, the intrinsic precursor dissipation behavior is equivalent across all samples within statistical variation. Figure 3(a) shows the average and standard error of the precursor dissipation as a function of cycle number for increasing maximum stress. These plots unambiguously demonstrate the training phenomenon: the precursor hysteresis decays with cycling. Increasing the maximum stress triggers new precursor avalanches and new training cycles. Below the catastrophic failure stress σ_c , the precursor dissipation virtually vanishes. Post the failure stress, the hysteretic dissipation continues beyond the prescribed 100 stress cycles, which indicates that the training is incomplete.

We characterize the decay of precursor dissipation, U, versus the number of cycles, n, using a fitting function $U_f(n)$ [8],

$$U_f(n) = (U_0 - U_{\infty})e^{-n/\tau}n^{-\delta} + U_{\infty},$$
 (1)

where $U_{\infty} = U_f(n \to \infty)$ is the estimated steady-state dissipation. U_0 is the initial dissipation. The power-law decay of U_f hints at the fluctuation behavior near the critical point. This analysis reveals that the catastrophic failure stress σ_c in these experiments can be associated with the RIT critical stress. This association is corroborated by the nonzero limiting dissipation U_{∞} for a maximum stress amplitude of $\sigma_{\text{max}} \geq \sigma_c$. We approximate the longterm decay at the step at $\sigma_{\rm max} \sim \sigma_c$ as critical behavior and fit the precursor dissipation U(n) using the simple powerlaw function, $U_f'(n) = U_f(n; \tau \to \infty, U_\infty \to 0) = U_0 n^{-\delta}$, and estimate the exponent δ be 0.68. A separate fit for δ at different maximum stresses gives an average exponent with standard deviation fluctuation $\delta = 0.70 \pm 0.18$. We apply the fitted power-law exponent $\delta = 0.70$ to determine τ for the remaining stress steps. Additional fitting details are provided in the Supplemental Material, Sec. S5.

We find, unlike granular systems [41] but like the colloidal systems, that the dislocation avalanches mostly disappear during the unloading branch (and hence, at the reversibility transition, also on the loading branch). This observed behavior could simply reflect a typical dislocation pinning stress large compared to the failure stress. Modifying the mean-field model, which studies hysteresis in a granular system [42], we incorporate the exponential decay rate τ , and predict $\delta = 1$ (see the Supplemental Material, Sec. S6, for details [27]). The

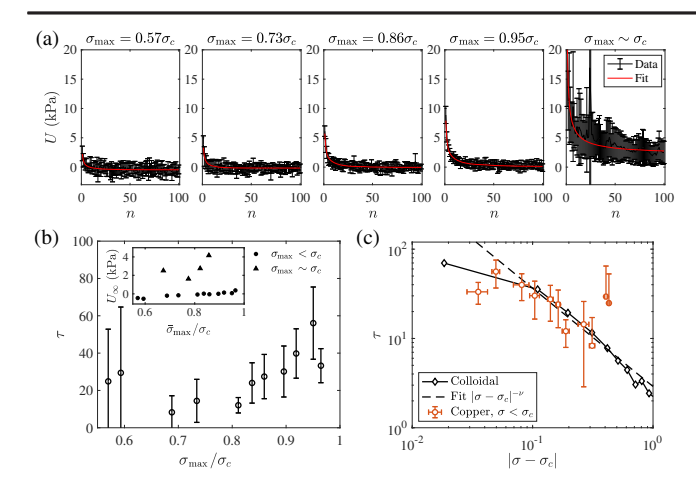


FIG. 3. Training experimental results showing precursor dissipation activity at different maximum stresses. (a) The precursor dissipation energy U at each representative maximum stress that shows its decay with the number of loading cycles, n. (b) Characteristic decay time τ versus the normalized maximum stress $\sigma_{\rm max}$ estimated for 3 $\mu{\rm m}$ diameter copper pillars. Inset shows that the estimated steady-state U_{∞} is close to zero below the critical stress σ_c and abruptly increases to ~2–4 kPa when $\sigma_{\rm max}$ reaches σ_c . The deviation of the final point in (b) and the corresponding points in (c) from the expected power-law divergence is probably due to our method for estimating the steady-state value (see the Supplemental Material, Sec. S7 [27]). (c) A direct comparison of dislocation RIT behavior gleaned from the Cu micropillar compression experiments with that reported for a colloidal particle system in a sheared suspension [8], which provides evidence for a divergence of necessary cycle time τ to reach a reversible state, close to the critical failure stress σ_c .

theoretical exponent, however, is far outside our statistical errors for the collective fit, but within the fluctuations for δ fit separately for different $\sigma_{\rm max}$.

Figure 3(b) shows that the decay time constant of precursor hysteresis τ increases with maximum stress $\sigma_{\rm max}$. The inset shows that the estimated steady-state U_{∞} is close to zero below the critical stress σ_c and abruptly increases to \sim 2–4 kPa when $\sigma_{\rm max}$ reaches σ_c [43]. Plotting the characteristic timescale, τ , as a function of proximity to critical point on a log-log scale in Fig. 3(c), we find a striking resemblance to the colloidal suspension systems, which indicates that stress-driven dislocations in smallscale metals exhibit RIT behavior similar to that seen in sheared colloidal particles [8]. Note that τ , which is related to the number of cycles in our experiments, is not a true timescale of the system. The deviation of the final point in Figs. 3(b) and 3(c) from the expected power-law divergence is probably due to our method for estimating the steadystate value (see the Supplemental Material, Sec. S7 [27]).

Analogous to the colloidal suspension systems, it is plausible that, at low stresses, the strongly interacting dislocations in the pillars may rearrange themselves into a stable configuration as the system reloads the first time. At higher peak stresses, the dislocation rearrangements in

one cycle may trigger a cascade of further avalanches in subsequent cycles. In small-scale crystalline plasticity, the RIT corresponds to the stress at which additional cycling continues to plastically deform the system with no additional applied forces, which corresponds to the failure stress. We can speculate about the relation between the critical behavior of the precursor avalanches observed here and the power-law distribution of dislocation avalanches observed in nano- and micropillars under monotonic loading. The precursor avalanches at an RIT usually diverge in size only near the failure stress. Plasticity avalanches under monotonic loading are debated to be associated with a "stress-tuned criticality" [44,45] or a jamming transition [46], either of which exhibit a power-law scaling with a cutoff in the avalanche size distribution that diverges only as the stress approaches the "failure stress"-precisely as one would expect for the approach to an RIT.

In this Letter, we bring attention to the overlooked signature of yield precursor avalanches in nanomechanical experiments. We show that the amount of dissipation due to yield precursor avalanches decays over repeated stress training cycles. We find that the characteristic decay time increases with the applied maximum stress. The apparent divergence of the time constant at a maximum stress near the quasistatic failure stress indicates that the flow transition of the dislocation system is fundamentally an RIT. This is the first time that this effect has been shown in any crystalline material experimentally. Prior studies have only focused on amorphous materials and attributed RIT behavior to many disordered or short-range ordered material systems. Our work extends the universality of RIT to include crystals. The training and RIT behavior has potential connections with cyclic fatigue and the transition from rapid hardening to saturation hardening at bulk scales, e.g., shakedown and ratcheting [47], wherein the dislocations microstructures evolve from mutual trapped bundles into distant loop patches [17,18]. However, we demonstrate that size effect is not negligible, which corroborates with the lack of prior research on training effects and precursor avalanches at large scales. Nanomechanical experiments have been intensively explored as a powerful methodology to study the fundamentals of crystal deformation, but the understanding of the dislocation plasticity in terms of RIT was hitherto lacking because people had only focused on quasistatic experiments which are not efficient in resolving history-dependent dissipative features of materials. Our Letter may inspire novel approaches to study plasticity, fatigue, and catastrophic failure in crystalline materials governed by complex dislocation dynamics.

J. R. G. and X. N. acknowledge financial support from the U.S. Department of Energy's Office of Basic Energy Sciences through Grant No. DESC0016945. J. P. S. and D. B. L. acknowledge the financial support of the U.S. Department of Energy's Office of Basic Energy Sciences through Grant No. DE-FG02-07ER46393 and NSF Grant No. DMR-1719490. K. A. D. acknowledges NSF Grant

No. CBET 1336634. We thank Stefano Zapperi, Giulio Costantini, D. Zeb Rocklin, Archishman Raju, and Lorien Hayden for helpful discussions.

- xni@northwestern.edu
- [1] M. D. Uchic, D. M. Dimiduk, J. N. Florando, and W. D. Nix, Science 305, 986 (2004).
- [2] J. R. Greer, W. C. Oliver, and W. D. Nix, Acta Mater. 53, 1821 (2005).
- [3] D. M. Dimiduk, C. Woodward, R. LeSar, and M. D. Uchic, Science 312, 1188 (2006).
- [4] M. C. Miguel, A. Vespignani, S. Zapperi, J. Weiss, and J.-R. Grasso, Nature (London) 410, 667 (2001).
- [5] J. Lubliner, *Plasticity Theory*, Dover books on engineering (Dover Publications, Mineola, 2008).
- [6] J. P. Sethna, M. K. Bierbaum, K. A. Dahmen, C. P. Goodrich, J. R. Greer, L. X. Hayden, J. P. Kent-Dobias, E. D. Lee, D. B. Liarte, X. Ni, K. N. Quinn, A. Raju, D. Z. Rocklin, A. Shekhawat, and S. Zapperi, Annu. Rev. Mater. Res. 47, 217 (2017).
- [7] D. Pine, J. Gollub, J. Brady, and A. Leshansky, Nature (London) 438, 997 (2005).
- [8] L. Corté, P. M. Chaikin, J. P. Gollub, and D. J. Pine, Nat. Phys. 4, 420 (2008).
- [9] I. Regev, J. Weber, C. Reichhardt, K. A. Dahmen, and T. Lookman, Nat. Commun. 6, 8805 (2015).
- [10] P. Leishangthem, A. D. S. Parmar, and S. Sastry, Nat. Commun. 8, 14653 (2017).
- [11] R. Jeanneret and D. Bartolo, Nat. Commun. 5, 3474 (2014).
- [12] K. Hima Nagamanasa, S. Gokhale, A. K. Sood, and R. Ganapathy, Phys. Rev. E 89, 062308 (2014).
- [13] M. C. Rogers, K. Chen, L. Andrzejewski, S. Narayanan, S. Ramakrishnan, R. L. Leheny, and J. L. Harden, Phys. Rev. E 90, 062310 (2014).
- [14] R. Möbius and C. Heussinger, Soft Matter 10, 4806 (2014).
- [15] S. Slotterback, M. Mailman, K. Ronaszegi, M. van Hecke, M. Girvan, and W. Losert, Phys. Rev. E 85, 021309 (2012).
- [16] C. Zhou, C. Olson Reichhardt, C. Reichhardt, and I. Beyerlein, Phys. Lett. A **378**, 1675 (2014).
- [17] J. C. Grosskreutz, Physica Status Solidi 47, 11 (1971).
- [18] Z. Basinski and S. Basinski, Prog. Mater. Sci. 36, 89 (1992).
- [19] R. Cleveland and A. Ghosh, Int. J. Plast. 18, 769 (2002).
- [20] Y. Xiang and J. Vlassak, Acta Mater. 54, 5449 (2006).
- [21] J. Brown and N. Ghoniem, Acta Mater. 58, 886 (2010).
- [22] R. A. Bernal, A. Aghaei, S. Lee, S. Ryu, K. Sohn, J. Huang, W. Cai, and H. Espinosa, Nano Lett. 15, 139 (2015).
- [23] J. Rajagopalan, J. H. Han, and M. T. A. Saif, Science 315, 1831 (2007).
- [24] D. Liu, Y. He, D. J. Dunstan, B. Zhang, Z. Gan, P. Hu, and H. Ding, Phys. Rev. Lett. 110, 244301 (2013).
- [25] X. Ni, S. Papanikolaou, G. Vajente, R. X. Adhikari, and J. R. Greer, Phys. Rev. Lett. 118, 155501 (2017).

- [26] M. Zaiser, Adv. Phys. 55, 185 (2006).
- [27] See Supplemental Material at http://link.aps.org/ supplemental/10.1103/PhysRevLett.123.035501 for additional information, which includes Refs. [28–36].
- [28] R. Maass, M. Wraith, J. T. Uhl, J. R. Greer, and K. A. Dahmen, Phys. Rev. E 91, 042403 (2015).
- [29] I. N. Sneddon, Int. J. Eng. Sci. 3, 47 (1965).
- [30] M. D. Uchic, P. A. Shade, and D. M. Dimiduk, Annu. Rev. Mater. Res. 39, 361 (2009).
- [31] Y. Cui, Z. Liu, and Z. Zhuang, Int. J. Plast. 69, 54 (2015).
- [32] A. T. Jennings, J. Li, and J. R. Greer, Acta Mater. **59**, 5627
- [33] P. K. Agnihotri and E. Van Der Giessen, Mech. Mater. 90, 37 (2015).
- [34] L. Nicola, Y. Xiang, J. J. Vlassak, E. Van der Giessen, and A. Needleman, J. Mech. Phys. Solids 54, 2089 (2006).
- [35] D. W. Marquardt, J. Soc. Ind. Appl. Math. 11, 431 (1963).
- [36] W. Press, B. Flannery, S. Teukolsky, and W. Vetterling, *Numerical Recipes* (Cambridge University Press, Cambridge, England, 1986), pp. 430–436.
- [37] F. F. Csikor, C. Motz, D. Weygand, M. Zaiser, and S. Zapperi, Science **318**, 251 (2007).
- [38] S. Brinckmann, J.-Y. Kim, and J. R. Greer, Phys. Rev. Lett. 100, 155502 (2008).
- [39] J. Weiss, W. B. Rhouma, T. Richeton, S. Dechanel, F. Louchet, and L. Truskinovsky, Phys. Rev. Lett. 114, 105504 (2015).
- [40] The perfect failure mode is not observed in the LC compression experiments because a dynamic increase in engineering stress is required to compensate for the plastic deformation induced contact area change of the pillar loaded in \langle 111 \rangle high-symmetry direction to maintain the true applied stress above the critical stress level.
- [41] R. García-Rojo, F. Alonso-Marroquín, and H. J. Herrmann, Phys. Rev. E 72, 041302 (2005).
- [42] M. M. Bandi, H. G. E. Hentschel, I. Procaccia, S. Roy, and J. Zylberg, Europhys. Lett. 122, 38003 (2018).
- [43] The true stress estimates are not reliable post the plastic collapse, as the true stress-strain conversion (see Supplemental Material, Sec. S1 [27]) holds only in the conditions that (i) the lattice orientation does not change significantly and that (ii) deformation remains approximately homogeneous on the pillar scale.
- [44] N. Friedman, A. T. Jennings, G. Tsekenis, J.-Y. Kim, M. Tao, J. T. Uhl, J. R. Greer, and K. A. Dahmen, Phys. Rev. Lett. 109, 095507 (2012).
- [45] K. A. Dahmen, Y. Ben-Zion, and J. T. Uhl, Phys. Rev. Lett. 102, 175501 (2009).
- [46] P. D. Ispánovity, L. Laurson, M. Zaiser, I. Groma, S. Zapperi, and M. J. Alava, Phys. Rev. Lett. 112, 235501 (2014).
- [47] S. Suresh, *Fatigue of Materials*, 2nd ed. (Cambridge University Press, Cambridge, England, 1998).